Editors' Suggestion

# Energy Fluctuations in Slowly Sheared Granular Materials

Jie Zheng,[1,*] Aile Sun,[1,*] Yujie Wang,[1] and Jie Zhang[1,2,3,†]
[1]School of Physics and Astronomy, Shanghai Jiao Tong University, Shanghai 200240, China
[2]Institute of Natural Sciences, Shanghai Jiao Tong University, Shanghai 200240, China
[3]Collaborative Innovation Center of Advanced Microstructures, Nanjing 210093, China

(Received 19 September 2018; published 10 December 2018)

Here we show the first experimental measurement of the particle-scale energy fluctuations $\Delta E$ in a slowly sheared layer of photoelastic disks. Starting from an isotropically jammed state, applying shear causes the shear-induced stochastic strengthening and weakening of particle-scale energies, whose statistics and dynamics govern the evolution of the macroscopic stress-strain curve. We find that the $\Delta E$ behave as a temperaturelike noise field, showing a novel, Boltzmann-type, double-exponential distribution at any given shear strain $\gamma$. Following the framework of the soft glassy rheology theory, we extract an effective temperature $\chi$ from the statistics of the energy fluctuations to interpret the slow startup shear (shear starts from an isotropically jammed state) of granular materials as an "aging" process: Starting below one, $\chi$ gradually approaches one as $\gamma$ increases, similar to those of spin glasses, thermal glasses, and bulk metallic glasses.

DOI: 10.1103/PhysRevLett.121.248001

Granular materials, such as sand, soil, wheat, and powders, are of tremendous importance in industrial applications and geophysical processes. One fascinating and deep statistical problem in granular physics is concerned with all sorts of strong fluctuations in granular materials subject to shear deformation. These fluctuations emerge at all spatial and timescales and are beyond the normal statistical mechanical description due to the highly dissipative nature of granular materials. Understanding the nature of the fluctuations is crucial to a number of geological and industrial applications, such as avalanches and earthquakes [1–3], and the breakdown of disordered materials, such as bulk metallic glasses [4–6], due to the close connection between the jammed and glassy materials [7]. Two profound physical questions arise naturally and remain to be investigated: (i) Is there a granular temperature to describe the statistics of these fluctuations [8]? (ii) How do these fluctuations connect to the behaviors of macroscopic variables of a system?

Extensive experimental and numerical works have been carried out to study the fluctuations of particle displacements, velocities [9–13] and rotations [14], strains [15,16], stress time series [17–19], drag forces [20–23], and boundary contact forces [24]. However, to our best knowledge, there exists no study of the particle-scale energy fluctuations because of the notorious difficulty of measuring particle-scale interactions. The characteristics and nature of the particle-scale energy fluctuations form the microscopic basis of a number of mesoscopic theories based on the local elasticity and yielding, including the shear transformation zone theories [4–6], the soft glassy rheology (SGR) theories [25–28], and the mean-field scaling theories [1,29]. The range of fluctuations is also relevant to a number of continuum descriptions of granular flows, such as the hydrodynamic descriptions [30,31] and the constitutive relations [32–35].

We perform the first experimental study of the particle-scale energy fluctuations $\Delta E$ in a slowly sheared dense packing of bidisperse photoelastic disks under a constant confining pressure, whose initial state is an isotropically jammed packing. We choose the startup shear (shear starts from an isotropically jammed state), because it is related to the plasticity of amorphous materials, which has become a paradise of intense research in recent years [4–6,25–28,36–43]. We find a novel, Boltzmann-type, double-exponential distribution of $\Delta E$ at every step of strain $\gamma$, which originated in the shear-induced stochastic strengthening and weakening in space. The spatial fluctuations of energies, $\Delta E$, show a weak correlation with local strain fields and relax rapidly like a $\delta$ function, acting as a temperaturelike noise field. The double-exponential distribution of $\Delta E$ yields two characteristic energy scales at every strain $\gamma$. Following the framework of the SGR theories [25–28], we define a dimensionless effective temperature $\chi$ that quantifies the competition between the small-scale shear-induced stiffening and weakening at a mean-field level. We can interpret the slow startup shear of granular materials as an "aging" process: Starting below one, $\chi$ gradually approaches one as $\gamma$ increases, similar to those of spin glasses [44] and thermal glasses [45]. In addition, this behavior of $\chi$ is consistent with the findings of the numerical study of a model metallic glass, in which mechanical failure is argued as the glass transition induced by applied shear stress [46].

Using a two-dimensional biaxial apparatus sketched in Fig. 1(a), we applied quasistatic pure shear to a rectangular frame, allowing the distance along the $y$ axis to relax under

 

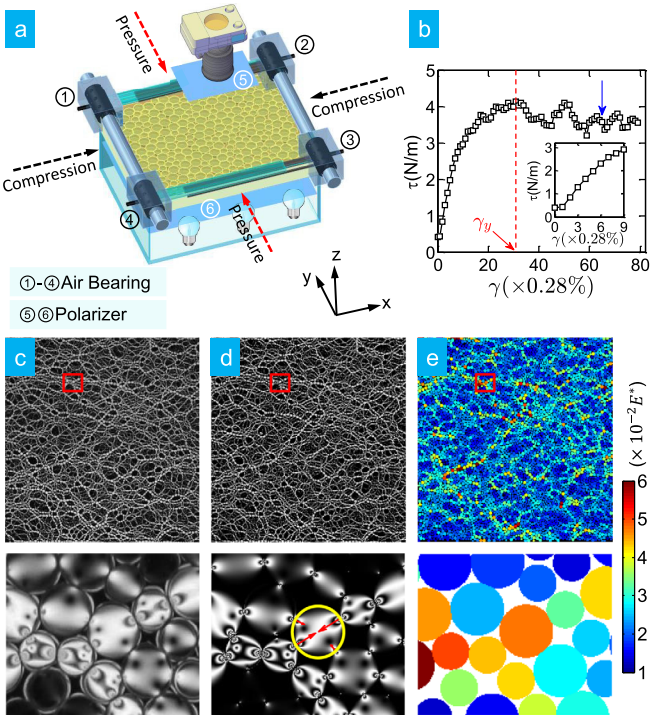


FIG. 1. (a) The schematic of the experimental setup. (b) A typical stress-strain curve. An inset shows the enlarged curve for $\gamma < 2.8\%$. A dashed line denotes the position of yield strain $\gamma_y$. A blue arrow labels the $\gamma$, where (c)–(e) are referring to. (c) An experimentally recorded image of force chains. (d) A computer-constructed image (upper panel) using the measured contact forces. The examples of measured contact forces are drawn using four red arrows on a yellow-circled disk in the lower panel. (e) The map of the measured particle-scale energies. The lower panels in (c)–(e) plot a magnified small portion of the force chain image, the corresponding computed constructed images of force chains, and the particle-scale energies, which correspond to the same group of particles labeled in those three red squares in the upper panels in (c)–(e).

a fixed confining pressure $P_y$. A layer of photoelastic disks, immersed in density-matched brine to eliminate the base friction, filled the rectangular frame randomly, with a size ratio of 0.7 cm/1.0 cm and a number ratio of 1:1 to avoid crystallization. The inertial number [34] is $\sim 10^{-5}$. The pure shear was applied in multiple steps with a step strain of $\delta\gamma = 2\delta L_x/L_{x0} = 0.28\%$, where $L_{x0}$ is the initial frame size along the $x$ axis and $2\delta L_x$ is the size change within one step. The two boundaries perpendicular to the $y$ axis were made of aluminum bars stacking on each other to allow a flexible boundary size during shear, whose two ends were attached to air bearings to achieve an accuracy of $P_y$ within 1%. We checked a range of system sizes from 500 to 7000 disks and observed no obvious finite-size effect for systems larger than 2000 disks. The frictional coefficient $\mu$ between disks is around 0.1. We also performed experiments using disks of a higher frictional coefficient ($\mu \sim 0.7$) and found no obvious qualitative changes. The disk layer was sandwiched between two circular polarizer sheets. For each of three different $P_y$ of 8.61, 10.04, and 11.48 N/m, we repeated experiments multiple times for better statistics. Since the results of different $P_y$ show no qualitative differences, here we present only the results of $P_y = 11.48$ N/m with a system size of 5260 disks.

We show a typical stress-strain curve $\tau(\gamma)$ in Fig. 1(b). When shear is applied to an isotropically jammed packing, $\tau$ increases almost linearly from zero; around $\gamma \approx 2\%$, $\tau$ starts increasing nonlinearly up to the yield strain $\gamma_y \approx 8.5\%$, where $\tau$ reaches a peak and above which $\tau$ gradually enters a steady state of random fluctuations. This behavior seems generic to those of other disordered systems, such as wet foams [47] and molecular glasses [43]. One central task of modern plasticity theories of disordered materials [4–6,25–28,36–43] is to connect this macroscopic behavior of $\tau(\gamma)$ to the microscopic internal processes of structural, stress, and energy relaxations, which is one of the goals of the present study.

The details of measuring the elastic energy $E_i$ of a disk $i$ are given in Supplemental Material [48]. Briefly, $E_i$ equals all the work done to deform the disk at its all contacts. At a contact, the work is computed by the integrals of the calibrated contact-force laws of the normal and tangential forces, since force is related to the gradient of work. Figure 1(e) shows the measured $E_i$ of all disks in a sample image based on the measurement of the contact forces, as shown in Figs. 1(c) and 1(d).

From the spatial distributions of $E_i$ at strains $\gamma$ and $\gamma + \delta\gamma$, we measure the particle-scale energy fluctuation $\Delta E \equiv E_i(\gamma + \delta\gamma) - E_i(\gamma)$ by tracking the energy change for each particle $i$. The results of $\Delta E$ at $\gamma = 0$, and $\Delta E$ at

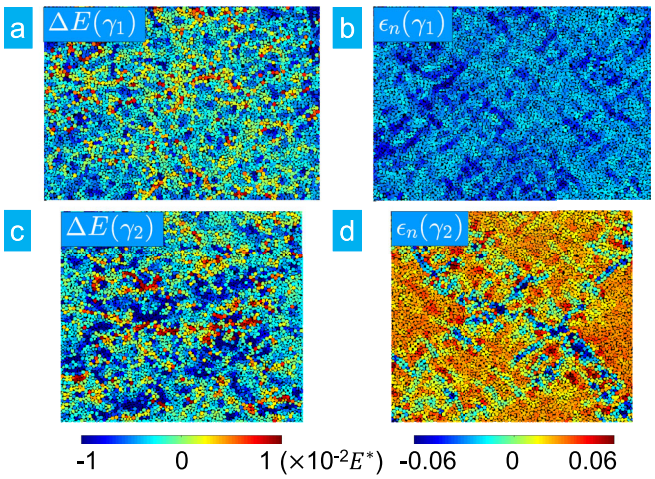


FIG. 2. The spatial maps of the energy fluctuations $\Delta E$ in (a) and the coarse-grained local diagonal strains $\epsilon_n \equiv \epsilon_{xx} - \epsilon_{yy}$ in (b). Here, at a given axial strain $\gamma$, $\Delta E(\gamma) \equiv E(\gamma + \delta\gamma) - E(\gamma)$. In the first row, $\gamma_1 = 0$, and in the second row, $\gamma_2 = 1.37\gamma_y$. The spatial features of local strain are nearly unobservable in the distributions of $\Delta E$. The $\Delta E$ are in units of $E^* \equiv P_y \times D^2$, where $P_y$ is the confining pressure and $D$ is the average particle diameter.

$\gamma > \gamma_y$, are shown in Figs. 2(a) and 2(c), which correlate weakly with the particle-scale strain fluctuations $\epsilon_n$ shown in Figs. 2(b) and 2(d). A quantitative correlation between the two is around 5% for all $\gamma$. Moreover, $\Delta E$'s are much smaller than $E^* \equiv P_y D^2$, where $D$ is the average disk diameter, as a result of energy changes at the contact levels. We believe that the stochastic energy fluctuations are connected to the evolution of the force-chain networks of jammed states under shear. Note that $P_y \sim 10$ N/m, which can be converted to a dimensionless pressure $\widetilde{P_y} \sim 0.1$ according to the standard procedure described in the literature [50], meaning that the packing is highly jammed [50]. Here $\widetilde{P_y}$ is defined as $P_y/(AD^{\alpha+1-d})$, where $A$ is the typical value of the normal spring constant, $D$ is the average disk diameter, $\alpha$ is the power exponent of the force law, and $d$ is the dimension. The values of $A$ and $\alpha$ can be obtained from the calibration of the force law of disks [see, e.g., Eq. (2) in Supplemental Material [48]]. Under the quasistatic shear, at every strain $\gamma$, the corresponding packing is under mechanical equilibrium of force-and-torque balances on every particle. The potential energy landscape (PEL) of a system has many local minima, similar to those of hard-sphere jamming [51], but with much more metastable configurations due to the friction at contacts. Since each local minimum corresponds to a jammed packing, the quasistatic shear explores continuously a sequence of densely distributed jammed states. The above argument is consistent with an early finding that a sheared granular material in a three-dimensional cell explores phase space as if it were an equilibrium system [24]. In real space, the change of the contact force network at the contact level (contact breaking or recreation, elastic loading, or microslipping) causes the stochastic strengthening and weakening of contact-level (hence, particle-scale) elastic energies. The shear-induced weakening happens even right at the beginning of the shear, where the $\tau(\gamma)$ increases linearly as already seen in Fig. 1(b). This observation is consistent with the previous theoretical studies of plasticity of molecular glasses [4–6] [25–28,36–43], in which the small-scale plasticity takes place much before a material yields. However, the weak correlation between $\Delta E$ and $\epsilon_n$ suggests that in granular materials the dominant contribution to the local energy drops comes from the contact levels, in contrast to those of molecular glasses that are caused by particle-scale rearrangements [4–6,25–28,36–43].

Despite the complex behaviors of $\Delta E$, at the mean-field level, their statistics and dynamics may be described using the thermodynamic concept of effective temperature [4–6,25,26,28,38]. Note that the "temporal" (in $\gamma$) autocorrelations $C(\Delta\gamma)$ of $\Delta E$ show a $\delta$-correlated sharp decay, whereas those of $\epsilon_n$ decay slowly, in a stretched exponential form, as seen in Fig. 3(a). The results and those in Fig. 2 strongly suggest that the energy fluctuations $\Delta E$ behave as a noise-temperature-like field.

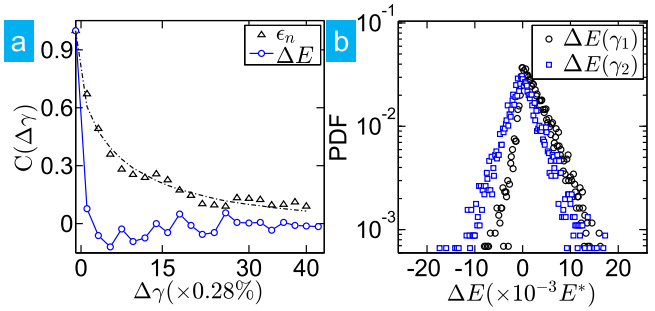


FIG. 3. The relaxations of energy fluctuations decay much more rapidly compared to those of strain in (a). In (a), the correlation functions $C(\Delta\gamma)$ of the energy fluctuations $\Delta E$ are nearly $\delta$ correlated, in a sharp contrast to that of the strain $\epsilon_n$, which can be fit well using a stretched exponential function (the dotted line). Here, $C(\Delta\gamma) \equiv \langle A(\gamma, \vec{r})A(\gamma + \Delta\gamma, \vec{r})\rangle$ for a variable $A$, in which the $\langle\rangle$ stands for the spatial average over different positions $\vec{r}$. The probability distribution functions (PDFs) of the energy fluctuations $\Delta E$ in (b) show a Boltzmann-type, double-exponential distribution for both $\Delta E > 0$ and $\Delta E < 0$, with $\mathrm{PDF}(\Delta E < 0) \sim \exp(-|\Delta E|/\alpha_-)$ and $\mathrm{PDF}(\Delta E > 0) \sim \exp(-|\Delta E|/\alpha_+)$. Results are shown for two different axial strains of $\gamma_1 = 0$ and $\gamma_2 = 1.37\gamma_y$.

The probability distribution function (PDF) of $\Delta E$ at any given $\gamma$ shows an asymmetric Boltzmann-type, double-exponential distribution for both $\Delta E > 0$ and $\Delta E < 0$, producing two separate energy scales of $\alpha_\pm(\gamma)$, as shown in Fig. 3(b). The exact cause of the double-exponential distribution of $\Delta E$ is not completely clear. However, the early experiment by Geng and Behringer may provide some clue, where they measured the time series of drag forces of a tracer particle embedded in a slow granular flow [20]. The statistics of avalanche size extracted from the time series obeys an exponential distribution, which was understood as a result of the random excitations of the force chains due to the interactions between the tracer particle and surrounding force-network environment [20]. Here, if every particle is treated as a tracer particle, we have an ensemble of particles probing the different structure disorders of the system at different locations. Hence, the exponential distributions can be understood following a similar argument [20]. The asymmetry of the distribution reflects the symmetry breaking due to the elastic loading and irreversible microslips at contacts or contact breaking. Incidentally, we find that the physical meaning and behaviors of $\alpha_\pm(\gamma)$ can be interpreted within the framework of the SGR theory [25,26,28], which extended Bouchaud's trap model [52] to formulate the shear of soft glassy materials as an activation process in the PEL, by replacing the thermal temperature [52] with an effective temperature due to mechanical noises. A brief introduction of the SGR theory is given in Supplemental Material [48].

Analogous to the SGR theories [25,26,28], the PDF ($\Delta E < 0$) measures the distribution of local activation energy, representing the probability of the system hopping

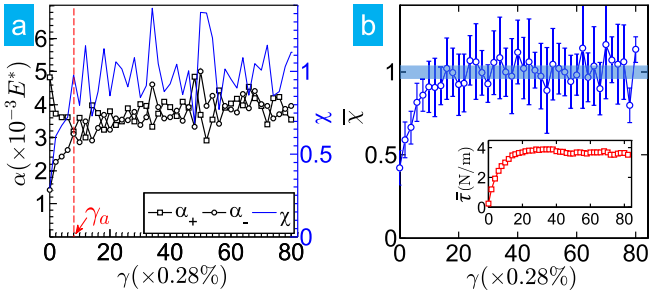


FIG. 4. The "aging time" $\gamma_a = 2.24\%$ is defined when the ratio $\chi \equiv \alpha_-/\alpha_+$, derived from the two energy scales $\alpha_\pm$, first approaches $\chi = 1$, as shown in (a). Beyond $\gamma_a$, the values of $\alpha_\pm$ become comparable, and thus the $\chi$ is pinned around $\chi \approx 1.0$. In SGR theories [25,26,28], when $\chi < 1$, the system is in the glassy state where the aging takes place. The $\alpha_\pm$ are obtained from the PDF of energy fluctuations $\Delta E$ as shown in Fig. 3(b). (b) shows the evolution of the ensemble-averaged effective temperature $\bar{\chi}$ (main panel) and the ensemble-averaged shear stress $\bar{\tau}$ (inset). The ensemble average is over ten different experimental runs under the same conditions.

out of a local minimum in the PEL, while the PDF($\Delta E > 0$) measures an *a priori* distribution of the local yield energy, representing the probability of the system hopping into the local minimum in the PEL. Here, we define $\chi \equiv \alpha_-/\alpha_+$ as a dimensionless temperature, analogous to that of the SGR theory [25,26,28]: When $\gamma < \gamma_a$, $\chi < 1$, analogous to the aging of glassy materials; when $\gamma \geq \gamma_a$, $\chi$ is "pinned" around the glass transition temperature $\chi \approx 1.0$ [25,26,28], as shown in Figs. 4(a) and 4(b). For all experimental runs, when $\gamma < \gamma_a$, $\alpha_-$ is systematically below $\alpha_+$. Intuitively, when shear starts, only the softest regimes yield before the tougher ones, leading to a monotonic increase of $\alpha_-$ from the lowest value; simultaneously, as $\alpha_-$ increases, the interaction causes the softening of stable regimes and, hence, a monotonic decrease of $\alpha_+$. Note that the aging time $\gamma_a < \gamma_y$ as seen in Fig. 4(b), which is consistent with the theoretical prediction of aging dynamics in the context of the SGR theory and the marginal dynamics in spin-glass theories [25,44] that the aging time usually sets other timescales of the system. In addition, the results in Fig. 4 are consistent with the early numerical simulations of thermal glasses [45], where the effective temperature approaches the glass transition temperature when the measured shear stress approaches a yield stress. Moreover, the results in Fig. 4 are consistent with the early numerical simulations of model metallic glasses [46], where mechanical failure is argued as the glass transition induced by applied shear stress. Compared to the evolution of the stress-strain curve $\tau(\gamma)$ in Fig. 1(b) and the ensemble-averaged curve $\bar{\tau}(\gamma)$ in the inset in Fig. 4(b), we see that the competition of $\alpha_-$ and $\alpha_+$ governs the evolution of the macroscopic stress-strain curve.

In summary, we have performed the first experimental measurement of the particle-scale energy fluctuations $\Delta E$ in slowly sheared granular materials under constant confining pressure. The spatial distributions of $\Delta E$ and local strain $\epsilon_n$ show weak spatial correlations during the shear deformation. The temporal correlations of $\Delta E$ decay sharply like a $\delta$ function, in contrast to the slow, stretched exponential decay of $\epsilon_n$. These observations suggest that $\Delta E$ behave as a temperaturelike noise field. In the mean-field level, we can understand the statistics and dynamical behaviors of $\Delta E$ in the framework of the soft glassy rheology theories by defining an effective temperature [25,26,28], which provides a unified description of the startup shear of granular materials and the aging of thermal glasses and soft glassy materials.

In fact, Edwards and Oakeshott first introduced an effective temperature to describe equilibrium statistics of granular packing [53]. In an ideal model granular system under uniform shear, theoretical studies suggested that an effective temperature could be extracted from the particle diffusivity and mobility and should be consistent with the Edwards temperature [8], which was supported by later experimental findings [54,55]. However, for systems with strong dynamical heterogeneity, such as ours, it is difficult to connect to the proposed theoretical picture [8] at the current stage. Recent studies uncovered deep connections between configurations of jammed packing and those of hard-sphere glasses and spin glasses [56]. The similarity between the evolution of $\chi$ in our experiment and those of spin glasses [44], thermal glasses [45], and metallic glasses [46] suggests that there exist profound connections in the dynamical evolution of phase-space configurations of these complex far-from-equilibrium systems.

J. Z. acknowledges support from the National Science Foundation of China under No. 11474196 and No. 11774221.

*These authors contributed equally.
†jiezhang2012@sjtu.edu.cn

[1] K. A. Dahmen, Y. Ben-Zion, and J. T. Uhl, Nat. Phys. **7**, 554 (2011).
[2] P. A. Johnson and X. Jia, Nature (London) **437**, 871 (2005).
[3] K. E. Daniels and N. W. Hayman, J. Geophys. Res. **113**, B11411, (2008).
[4] M. L. Falk and J. S. Langer, Annu. Rev. Condens. Matter Phys. **2**, 353 (2011).
[5] J. S. Langer, Phys. Rev. E **77**, 021502 (2008).
[6] M. L. Falk and J. S. Langer, Phys. Rev. E **57**, 7192 (1998).
[7] A. J. Liu and S. R. Nagel, Nature (London) **396**, 21 (1998).
[8] H. A. Makse and J. Kurchan, Nature (London) **415**, 614 (2002).
[9] B. Kou, Y. Cao, J. Li, C. Xia, Z. Li, H. Dong, A. Zhang, J. Zhang, W. Kob, and Y. Wang, Nature (London) **551**, 360 (2017).
[10] W. Losert, L. Bocquet, T. C. Lubensky, and J. P. Gollub, Phys. Rev. Lett. **85**, 1428 (2000).
[11] T. Miller, P. Rognon, B. Metzger, and I. Einav, Phys. Rev. Lett. **111**, 058002 (2013).

[12] J. R. Royer and P. M. Chaikin, Proc. Natl. Acad. Sci. U.S.A. **112**, 49 (2015).
[13] B. Utter and R. P. Behringer, Phys. Rev. E **69**, 031308 (2004).
[14] M. Harrington, M. Lin, K. N. Nordstrom, and W. Losert, Granular Matter **16**, 185 (2014).
[15] A. Amon, V. B. Nguyen, A. Bruand, J. Crassous, and E. Clement, Phys. Rev. Lett. **108**, 135502 (2012).
[16] A. Le Bouil, A. Amon, S. McNamara, and J. Crassous, Phys. Rev. Lett. **112**, 246001 (2014).
[17] R. P. Behringer, D. Bi, B. Chakraborty, S. Henkes, and R. R. Hartley, Phys. Rev. Lett. **101**, 268301 (2008).
[18] K. E. Daniels and R. P. Behringer, Phys. Rev. Lett. **94**, 168001 (2005).
[19] R. Hartley and R. Behringer, Nature (London) **421**, 928 (2003).
[20] J. Geng and R. P. Behringer, Phys. Rev. E **71**, 011302 (2005).
[21] K. Nichol, A. Zanin, R. Bastien, E. Wandersman, and M. van Hecke, Phys. Rev. Lett. **104**, 078302 (2010).
[22] K. A. Reddy, Y. Forterre, and O. Pouliquen, Phys. Rev. Lett. **106**, 108301 (2011).
[23] H. Zheng, D. Wang, J. Bares, and R. P. Behringer, Phys. Rev. E **98**, 010901 (2018).
[24] E. I. Corwin, H. M. Jaeger, and S. R. Nagel, Nature (London) **435**, 1075 (2005).
[25] S. M. Fielding, P. Sollich, and M. E. Cates, J. Rheol. **44**, 323 (2000).
[26] P. Sollich, F. Lequeux, P. Hébraud, and M. E. Cates, Phys. Rev. Lett. **78**, 2020 (1997).
[27] G. Picard, A. Ajdari, F. Lequeux, and L. Bocquet, Eur. Phys. J. E **15**, 371 (2004).
[28] P. Sollich, Phys. Rev. E **58**, 738 (1998).
[29] J. Lin, E. Lerner, A. Rosso, and M. Wyart, Proc. Natl. Acad. Sci. U.S.A. **111**, 14382 (2014).
[30] L. Bocquet, W. Losert, D. Schalk, T. C. Lubensky, and J. P. Gollub, Phys. Rev. E **65**, 011307 (2001).
[31] G. MiDi, Eur. Phys. J. E **14**, 341 (2004).
[32] M. Bouzid, M. Trulsson, P. Claudin, E. Clement, and B. Andreotti, Phys. Rev. Lett. **111**, 238301 (2013).
[33] D. L. Henann and K. Kamrin, Proc. Natl. Acad. Sci. U.S.A. **110**, 6730 (2013).
[34] P. Jop, Y. Forterre, and O. Pouliquen, Nature (London) **441**, 727 (2006).
[35] K. Kamrin and G. Koval, Phys. Rev. Lett. **108**, 178301 (2012).
[36] H. G. E. Hentschel, S. Karmakar, E. Lerner, and I. Procaccia, Phys. Rev. E **83**, 061101 (2011).
[37] R. Dasgupta, H. G. Hentschel, and I. Procaccia, Phys. Rev. Lett. **109**, 255502 (2012).
[38] A. Lemaitre, Phys. Rev. Lett. **89**, 195503 (2002).
[39] A. Lemaitre and C. Caroli, Phys. Rev. Lett. **103**, 065501 (2009).
[40] C. E. Maloney and A. Lemaitre, Phys. Rev. E **74**, 016118 (2006).
[41] C. Maloney and A. Lemaitre, Phys. Rev. Lett. **93**, 195501 (2004).
[42] A. Nicolas, J. Rottler, and J. L. Barrat, Eur. Phys. J. E **37**, 50 (2014).
[43] A. Tanguy, F. Leonforte, and J. L. Barrat, Eur. Phys. J. E **20**, 355 (2006).
[44] L. F. Cugliandolo and J. Kurchan, Phys. Rev. Lett. **71**, 173 (1993).
[45] T. K. Haxton and A. J. Liu, Phys. Rev. Lett. **99**, 195701 (2007).
[46] P. Guan, M. Chen, and T. Egami, Phys. Rev. Lett. **104**, 205701 (2010).
[47] J. Lauridsen, M. Twardos, and M. Dennin, Phys. Rev. Lett. **89**, 098303 (2002).
[48] See Supplemental Information at http://link.aps.org/supplemental/10.1103/PhysRevLett.121.248001 for additional experimental details and a brief introduction to the SGR theory, which includes Ref. [49].
[49] T. S. Majmudar and R. P. Behringer, Nature (London) **435**, 1079 (2005).
[50] C. S. O'Hern, L. E. Silbert, A. J. Liu, and S. R. Nagel, Phys. Rev. E **68**, 011306 (2003).
[51] S. Martiniani, K. J. Schrenk, K. Ramola, B. Chakraborty, and D. Frenkel, Nat. Phys. **13**, 848 (2017).
[52] C. Monthus and J.-P. Bouchaud, J. Phys. A **29**, 3847 (1996).
[53] S. F. Edwards and R. Oakeshott, Physica (Amsterdam) **157A**, 1080 (1989).
[54] C. Song, P. Wang, and H. A. Makse, Proc. Natl. Acad. Sci. U.S.A. **102**, 2299 (2005).
[55] J. Geng and R. P. Behringer, Phys. Rev. Lett. **93**, 238002 (2004).
[56] A. Baule, F. Morone, H. J. Herrmann, and H. A. Makse, Rev. Mod. Phys. **90**, 015006 (2018).